

# Inferring Changes in Intrinsic Parameters From Motion Blur

Alastair Barber<sup>a,b,\*</sup>, Matthew Brown<sup>a</sup>, Paul Hogbin<sup>b</sup>, Darren Cosker<sup>a</sup>

<sup>a</sup>Centre for Digital Entertainment, Computer Science, University of Bath, Bath, UK

<sup>b</sup>Double Negative Visual Effects, 160 Great Portland St., London, UK

---

## Abstract

Estimating changes in camera parameters, such as motion, focal length and exposure time over a single frame or sequence of frames is an integral part of many computer vision applications. Rapid changes in these parameters often cause motion blur to be present in an image, which can make traditional methods of feature identification and tracking difficult. In this work we describe a method for tracking changes in two camera intrinsic parameters - *shutter angle* and scale changes brought about by changes in *focal length*. We also provide a method for estimating the expected accuracy of the results obtained using these methods and evaluate how the technique performs on images with a low depth of field, and therefore likely to contain blur other than that brought about by motion.

---

## 1. Introduction

Estimating motion of a camera system, both in terms of *extrinsic* (camera movement relative to the world coordinate system) and *intrinsic* camera changes (such as changes in focal length) is an important aspect of many computer vision applications. Accurate estimation of these changes throughout a film sequence is an essential part of the Visual Effects (VFX) process, as without this information, computer generated assets, such as characters, scenery and effects, cannot be applied convincingly to live-action footage. Often, in order to determine changes in the camera parameters, it is necessary to track individual feature points over two or more frames after filming has taken place, or use additional camera mounted hardware such as a motion capture rig, inertial measurement devices, and other devices for tracking physical changes to the lens parameters. Commonly, the process of determining changes in camera parameters after filming is referred to as *match-moving*. This is a process that uses structure-from-motion computer vision techniques to estimate both camera motion and 3D scene structure using corresponding feature points over multiple frames [13, p. 207]. This process can often be time-consuming, and require the input of a skilled operator in order to produce an accurate camera track from even automatically detected and matched feature points. In the case of using additional hardware, this presents challenges such as gaining acceptance on set for installation, and the additional expense of equipment and operation. There are also often many situations where such equipment would be impractical - such as outdoors

or at sea, due to the reliance on additional infrastructure. However, recent developments in electromechanical sensors has allowed for the manufacture of gyroscopes and accelerometers that are both low cost and small. These devices are now starting to be included within cameras and can easily be mounted to them in order to provide information about their motion during filming. Examples of applications of such camera mounted devices range from assisting determining scene geometry [11] to correcting for distortions introduced by motion and camera rolling shutter [5]. One of the most significant challenges with using inertial measurement sensors to measure motion of the camera is that only changes in acceleration or rotational velocity are recorded. This can lead to significant errors in determining absolute position by integrating this data [12], and as such are rarely suitable for tracking camera motion when used alone. Devices which track physical changes in lens parameters are now commonly used in production environments and have gained acceptance across the industry - however they must be accurately synchronised to the video captured by the camera. Whilst this is now a quick process, occasionally it may not be completed correctly (if at all) for each shot, and manual alignment of the data in post-production is a time consuming and hence expensive task.

Accurate feature tracking is a reliable method of determining accurate camera motion estimations, and is an active area of research. However, there are several cases where it is difficult to get an accurate track, most noticeably when there is a fast unpredictable motion of the camera, which also often leads to a considerable amount of motion blur being present in a frame, making features undetectable. Another common method for determining camera movements is to make use of a method known as ‘Optical Flow’ across an image. In this process, a dense correspondence for each pixel across two frames is calcu-

---

\*Corresponding Author

Email addresses: a.e.barber@bath.ac.uk (Alastair Barber), m.brown@bath.ac.uk (Matthew Brown), hogbin@dneg.com (Paul Hogbin), dpc@cs.bath.ac.uk (Darren Cosker)

67 lated. Assuming that there are a sufficient number of sta-  
68 tionary objects in the scene, the camera's movement can  
69 be calculated using this correspondence information. Sim-  
70 ilarly to automatic feature detection and matching, the  
71 process of calculating the optical flow across frames also  
72 suffers from degradation in the presence of large quantities  
73 of motion blur.

74 In [17], the authors present a method for determin-  
75 ing dense optical flow in the presence of spatially-varying  
76 motion blur. This method produces good results, how-  
77 ever calculating optical flow over an entire image can be  
78 a computationally expensive process. In [6], the authors  
79 present a method of determining in real-time and using a  
80 single motion-blurred frame, an estimate for camera ro-  
81 tation - using characteristics of the motion blur directly,  
82 and without selecting or matching any features from the  
83 image.

84 In our previous work [1], we used motion blur induced  
85 onto an image by changes in focal length and camera ro-  
86 tation to track changes in two camera intrinsic parameters  
87 - namely focal length and shutter angle. We used accu-  
88 rate hardware tracking of changes in camera parameters  
89 (the focal length change of a lens and camera rotation) to  
90 gather ground truth datasets and validate our algorithms.  
91 We also demonstrated how, in a situation where unsyn-  
92 chronised data from certain sensors was available along-  
93 side blurred footage, the blur patterns from frames in this  
94 footage could be used to accurately synchronise the exten-  
95 sional data with camera frames. One of the main limitations  
96 of the approach presented in [1] is that in order for an accu-  
97 rate estimate of focal length to be produced, there must be  
98 a sufficient amount of motion-induced blur present in the  
99 frame, along with sufficient visual texture (in this case,  
100 sharp edges). In the following sections, we give an ex-  
101 panded description of our method as presented in [1] for  
102 determining shutter angle and scale change brought about  
103 by focal length change. In addition to this, we present  
104 an extension to this method for validating the accuracy of  
105 such results across two new datasets in differing conditions.  
106 We also investigate the effects of a shallow depth-of field  
107 (and hence images likely to contain a significant amount  
108 of blur irrespective of motion) on both our method.

## 109 2. Background

110 Our main motivation for this work is to improve the  
111 process of 'Matchmoving' for use in Visual Effects. In par-  
112 ticular, we are interested in accurately estimating changes  
113 in camera parameters automatically and from scenes that  
114 would cause traditional structure from motion techniques  
115 based upon feature detection and matching to fail. Motion  
116 blur is often present in footage, and it is not uncommon for  
117 it to be considered a desirable artistic effect by directors  
118 in order to convey a sense of fast movement to the viewer  
119 [4]. This can often present challenges in determining an  
120 accurate camera track [13, pp140-143], as many current  
121 techniques for feature identification and matching rely on

122 there being sharp corners or changes in image intensity  
123 being visible. Motion blur severely reduces the occurrence  
124 of these in an image. However, recent work has looked  
125 at using the characteristics of induced motion blur alone  
126 to determine parameters of a scene in order to avoid this  
127 limitation.

128 Using Motion blur directly to determine parameters  
129 of a scene is an area of current computer vision research.  
130 [9] presents a method of determining speed of a moving  
131 vehicle from a blurred image, whilst then using this infor-  
132 mation to de-blur the resulting image. Other methods,  
133 such as the one presented by Rekleitis [14] use the di-  
134 rection and magnitude of motion blur in the process of  
135 estimating optical flow in an image. Later work, in [17],  
136 parameterises each frame as a function of both pixel move-  
137 ment and motion-blur. In [17], the authors determine the  
138 derivative of the blurred frame with respect to both the  
139 motion and the blur, where the blur itself is a function  
140 of motion. Furthermore, if the exposure time is known as  
141 a fraction of the frame (*shutter angle*), the result can be  
142 further optimised. Recent work in [7] makes use of data  
143 captured from a 3D pose and position tracker attached to  
144 the camera to aid in the calculation of optical flow in im-  
145 ages affected by motion blur. As the level of motion blur in  
146 an image is typically directly related to the exposure time  
147 of the frame, [10] and [16] use a method with a hybrid  
148 camera capturing both high and low frame-rate images of  
149 the same scene to correct images exhibiting motion blur.

150 Presented by Klein and Drummond in [6] is a method  
151 for determining the rotation of a camera during a single-  
152 frame exposure resulting in motion blur. In this work,  
153 the axis of rotation is derived by selecting a point through  
154 which the most normals to the edgels at a set of 'edgel'  
155 (points along an edge) points coincide. This algorithm  
156 builds on the observation that areas of motion blur will  
157 typically form edges in the image. Figure 1 shows a syn-  
158 thetic animation that has undergone motion blur whilst  
159 the virtual camera has been rotated, and the results of  
160 this image having undergone Canny edge detection.

161 In the case of the scene in figure 1, the algorithm de-  
162 scribed in [6] will estimate the centre of rotation to be at  
163 the centre of the image plane - the *Z* axis. In order to  
164 handle rotations around the *X* and *Y* axis, the normal  
165 line to the edge at each edgel site is expressed as the inter-  
166 section of the image plane with a plane passing through  
167 the origin and and edgel site. Once the centre for rotation  
168 has been accurately determined using RANSAC (and opti-  
169 mised using a Levenberg-Marquardt based algorithm), the  
170 magnitude of rotation can be determined from analysing  
171 the blur along its direction, with the intensity of pixels in  
172 the image being sampled in concentric circles centred at  
173 the estimated axis of rotation. In [6], rotation magnitude  
174 is estimated under the assumption that the blur length  
175 cannot exceed the shortest intensity ramp produced by an  
176 intensity step in the scene (i.e., the least blurred feature).  
177 Under the further assumption that the largest intensity  
178 step in each scene will span approximately the same in-

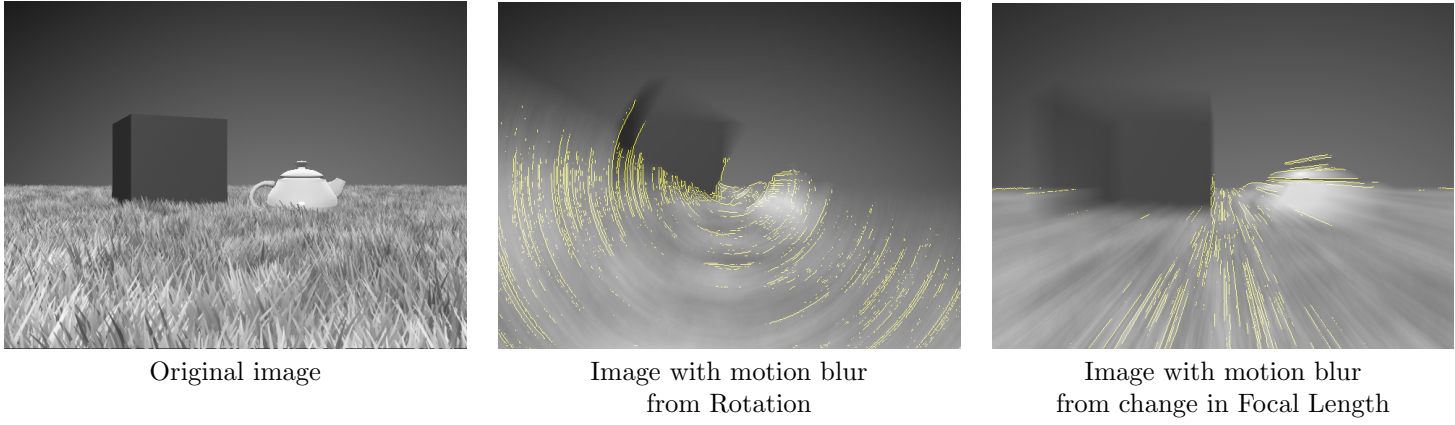


Figure 1: Images Blurred from Camera Rotation and Focal Length Changes with Resulting Canny Edge Detection

179 tensity increase, the gradient of the steepest ramp to span  
 180 this increase will therefore be inversely proportional to the length of the motion blur, and thus the magnitude of  
 181 rotation from the camera. Their work highlights a number  
 182 of important limitations in using motion blur to determine  
 183 changes in camera parameters, most notably that from a  
 184 single frame alone, it is not possible to determine the di-  
 185 rection (or sign) of rotation. For this reason, it is only  
 186 possible to compare the results of this algorithm with nor-  
 187 malised values of rotation from a rate-gyroscope or other  
 188 method for determining ground truth.

### 190 2.1. Intrinsic Parameters

191 The intrinsic parameters we consider in this work are  
 192 *focal length* and *shutter angle*.

193 If the focal length of a lens were to change whilst the  
 194 sensor or film is exposed, it could be expected that the  
 195 image will experience motion blur in a similar fashion to  
 196 those described in the previous section due to changes in  
 197 the field of view. An example of such an image is also  
 198 shown in Fig. 1. Although the entire image has been  
 199 scaled by a single value, it is apparent that different parts  
 200 of the image are blurred by differing amounts, specifically  
 201 - towards the centre of the image edges will still appear  
 202 sharper, despite being scaled, than towards the outside. It  
 203 is also clear that the ‘edges’ introduced by this blur con-  
 204 verge towards the centre of the image, in a similar fashion  
 205 to a translation of the camera originating from the centre  
 206 of the image.

207 When a frame is captured, the image sensor, or film,  
 208 is exposed for a short amount of time. Often, this amount  
 209 of time is known and controlled by the camera operator  
 210 - however there are occasions where this would be an un-  
 211 known value, such as in cameras with an automatically  
 212 controlled exposure. Fig. 2 shows two extracts from two  
 213 video sequences of a ball falling under gravity. The left  
 214 hand panel is a frame from a sequence shot with an ex-  
 215 posure time of 1/500th of a second, whilst the right hand  
 216 panel shows a similar scene captured with an exposure  
 217 time of 1/100th of a second. In both frames, the ball falls



Figure 2: Illustration of Shutter Angle and Motion Blur (25fps)

218 at an identical speed, and in both cases the *frame rate*  
 219 was set to 25 frames per second. Therefore, the left frame  
 220 would be exposed for  $\frac{1}{500} \div \frac{1}{25} = 0.05$  of the frame time and  
 221 the right hand frame for  $\frac{1}{100} \div \frac{1}{25} = 0.25$ . It can be seen  
 222 from Fig. 2, the frame with the longer exposure time as  
 223 a fraction of the frame exhibits the largest amount of mo-  
 224 tion blur. Historically, this fraction of time for which the  
 225 frame is exposed is determined by the *shutter angle*. This  
 226 is so called as in cameras with mechanical shutters con-  
 227 sisting of a rotating disk with an adjustable sector with  
 228 which to expose the film, the shutter angle referred to  
 229 the angle of opening of this sector. In the example from  
 230 Fig. 2, the shutter angle of the second frame would be  
 231  $360^\circ \times 0.25 = 90^\circ$ , and a frame for which the exposure  
 232 time is half the frame time would be  $180^\circ$ . Throughout  
 233 this work, for simplicity, we refer to the values for shutter  
 234 angles as fractions of the frame time.

## 235 3. Method

### 236 3.1. Measuring Focal Length Change from a Single Frame

237  
 238 In the case of a single motion-blurred frame undergoing  
 239 rotation, we use Klein and Drummond’s original method  
 240 to calculate the rotation,  $R$  around a 3D axis for that  
 241 frame. In our work, we focus on scale change in the 2D  
 242 image coordinate system. We also extend this method to  
 243 determine a scale change brought about by a change in  
 244 focal length without other motion. In our work, we focus

245 on a scale change taking place in the 2D image plane, with  
 246 the principal point of the lens being at the centre of the  
 247 image.

As shown in Fig. 1, the change in focal length (assuming the camera is not rotating or translating) adds motion blur to the image in a fashion similar to a translation towards the principal point of the image plane. Unlike the method used by Klein & Drummond to estimate for rotation, there is no need to determine the centre of the transformation as we can assume that the direction of the blur will always be towards the principal point of the image plane. Therefore, in order to determine the magnitude of blur, the intensity  $I$  of the image along several radial lines  $L$ , is sampled from the edge of the image inwards (Fig 3). The number of radial lines depends on the size of the image, and are sampled starting at locations on the edges of the image spaced 10 pixels apart. Therefore, for a  $640 \times 480$  image, there would be  $2 \times 64 + 2 \times 48$  lines sampled. This profile is then searched for the first occurrence of an intensity step change greater than a threshold value - and the length of this change (and image position of the start and end) is recorded. In a similar fasion to the authors of [6], we choose a threshold value in order to avoid under-estimating the length of the blur, and only consider ramps which span a large intensity change (over 50 grayscale levels) in order to detect large isolated intensity steps (representing edges) in the image. The first occurrence of the step-change is selected because edges are expected to be less blurred towards the centre of the image, and hence the shortest intensity ramp will always correspond to a minimally blurred edge towards the centre of the centre of the image. Unless the scale change is very large, the likelihood is that this edge towards the centre of the image will not have been affected by the scale change or motion blur, and will therefore represent a scale change of zero, regardless of the true change in scale. As the origin of the scale change will be the centre of the image Eqn.1 describes this relationship between an image point  $u$  and the point  $u'$  after a change in focal length  $f$ :  $\Delta f$ .

$$\begin{aligned} u &= f \frac{X}{Z} \\ u' &= (f + \Delta f) \frac{X}{Z} \\ \frac{u'}{u} &= 1 + \frac{\Delta f}{f} \end{aligned} \quad (1)$$

248 Where  $X$  is a scene point of distance  $Z$  from the front  
 249 nodal point of a lens.

250 Figure 3 shows the location of a blur region as detected  
 251 by this algorithm in a synthetically blurred image, and Fig.  
 252 4 the locations of all blur regions over the image.

253 After a pair of points has been obtained for each ra-  
 254 dial line, a RANSAC based algorithm is used in order to  
 255 determine the geometric transformation between the sets  
 256 of points. In this process, the start and end points of the  
 257 maximum gradient ramps from the radial search lines are

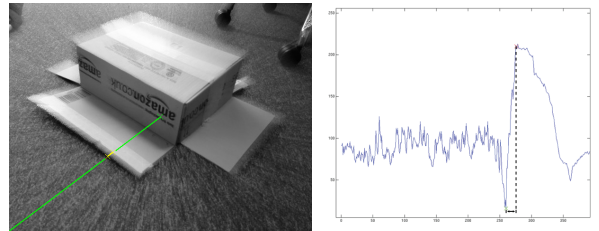


Figure 3: A line sample location (left) and profile (right). The peak gradient has been highlighted and location marked on the image.

258 represented as their respective image coordinates. The ge-  
 259 ometric transform brought about by a change in scale is  
 260 then estimated to produce an estimate of the scale trans-  
 261 form, using the points identified at each radial line. To  
 262 achieve this, we adapt the standard RANSAC algorithm  
 263 to take into account the observation that measuring the  
 264 magnitude of motion blur by searching for the maximal  
 265 gradient ramp will always produce an overestimate for the  
 266 blur magnitude. This would be because even in the case  
 267 where there is no blur, the sharpest edge might be sev-  
 268 eral pixels in extent, and in practice, in an image with  
 269 moderate motion blur, will extend several pixels beyond  
 270 the blurred region. Because of this, the error metric used  
 271 in the RANSAC based geometric estimation is weighted  
 272 to apply a higher penalty to estimations that produce an  
 273 under-estimate of the scale magnitude. This is done by  
 274 changing the model of our system in order to achieve a  
 275 result that match with the assumption that measuring the  
 276 length of a blurred edge will result in an over-estimate of  
 277 the true scale change.

278 In this process, instead of finding a hypothesis to max-  
 279 imise the number of start and end points for blur that  
 280 comply with  $((r' - r)^2 < \epsilon^2)$  where  $r'$  and  $r$  are the mea-  
 281 sured and predicted radial displacements, we maximise  
 282  $\sum((r' - (r + \epsilon))^2 < \epsilon^2)$ . By using this method, in or-  
 283 der to be considered an inlier,  $r'$  must be in the range  $r$   
 284 to  $r + 2\epsilon$ , as opposed to  $r - \epsilon < r' < r + \epsilon$  as in a tradi-  
 285 tional RANSAC procedure. The upper limit of this range:  
 286  $r + 2\epsilon$  was chosen as a limit arbitrarily and produces good  
 287 results, however it should be noted that other values, or  
 288 the use of methods such as Least Median Square estimate,  
 289 or MLESAC could be used to determine this value, al-  
 290 though these are not evaluated in this work. This method  
 291 provides an accurate estimate of the transformation be-  
 292 tween the points - whilst also rejecting outliers in the sets  
 293 of points.

294 As described in Section 2.1, the shutter of the camera  
 295 will only be open for a fraction of the frame time depending  
 296 on the *shutter angle*. The estimate for scale change from  
 297 motion blur will only take into account the time for which  
 298 the shutter was open, and not the overall frame.

### 299 3.2. Measuring Rotation Between Two Frames

300 The optical flow of two motion-blurred images can be  
 301 calculated using the baseline method described in [17].



Figure 4: Blur length estimation along all radial lines

302 Then, a set of feature points in the first frame are sampled  
 303 using [15], and their flow vectors used to calculate corre-  
 304 sponding points. As it is expected that there will be some  
 305 outliers, we use a RANSAC algorithm similar to that de-  
 306 scribed in Klein & Drummond to determine a consensus  
 307 set of matching points, in order to determine rotation. As  
 308 suming a correct pair of point matches,  $\hat{p}_1$  and  $\hat{p}_2$ , where  
 309  $\hat{p} = [x, y, 1]^T$  is a homogeneous point in the image coordi-  
 310 nate system, the line joining these points will be described  
 311 as  $L_p = \frac{\hat{p}_1 \times \hat{p}_2}{|\hat{p}_1 \times \hat{p}_2|}$ . As  $\hat{p}_1$  and  $\hat{p}_2$  are homogeneous coordi-  
 312 nates, the line  $L = (a, b, c)^T$  for which a point  $\hat{p} = (x, y, z)$   
 313 lies on is specified by the equation  $ax + by + cz = 0$ . As-  
 314 suming a further pair of correct point matches is available,  
 315 and the normal line to these can be calculated, the point of  
 316 intersection of these two normal lines ( $L_1$  and  $L_2$ ) should  
 317 then be the centre of rotation. This is where using the  
 318 homogeneous coordinate system is useful, as if the cam-  
 319 era is rotating around a point not in the image plane (for  
 320 example, its  $x$  or  $y$  axes, the centre of rotation can still  
 321 be represented in the image coordinate system, as the two  
 322 normal lines from point estimates would cross at infinity,  
 323 a point which can be represented in homogeneous image  
 324 coordinates as  $\hat{p} = (x, y, 0)^T$ .

325 Candidate point pairs and the best estimate for rota-  
 326 tion are selected using RANSAC. In this process, a pair of  
 327 candidate points and their matches are selected, and the  
 328 centre for rotation,  $C$  is calculated based on the method  
 329 described above. The connecting line for every other point  
 330 match is calculated, and the normal at the midpoint to this  
 331 line  $L_N$ , along with the line  $L_C$  from this midpoint to the  
 332 centre estimate, is calculated for each point pair. This is  
 333 illustrated in Fig. 5. The angle between the line  $L_N$  and  
 334  $L_C$ ,  $\theta$ , is calculated for each point pair - and capped at a  
 335 threshold value  $\epsilon$ . In this work the value for  $\epsilon$  is small, at  
 336 5 degrees, however should be varied by the user depend-  
 337 ing on the amount of candidate points expected (which  
 338 can depend on the visual texture of a scene) and expected  
 339 rotation magnitude.

340 The centre estimate producing the lowest sum of these  
 341 angles is then selected as the rotation centre. This point

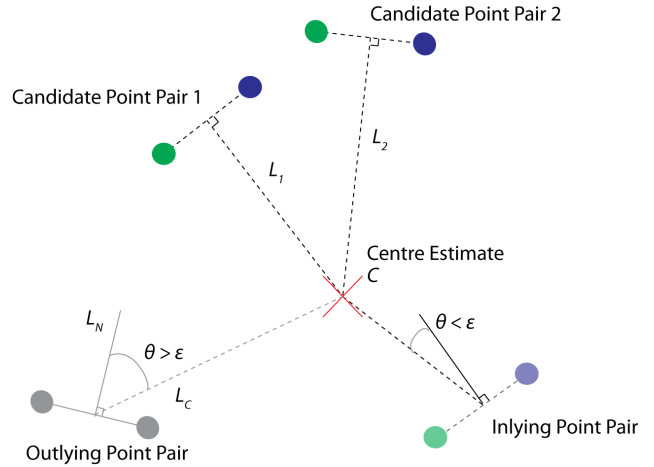


Figure 5: Illustration of Estimating the Centre of Rotation from Point Match Pair Candidates

342 is then normalised, and it's coordinates  $C = (x, y, z)^T$   
 343 treated as a 3D point. The Least Mean Squared value  
 344 for the angle between this point and the centre points  
 345 between inlying point match pairs is then treated as the  
 346 frame-to-frame rotation magnitude. Results obtained us-  
 347 ing this method alongside Klein and Drummond's single  
 348 frame method - using synthetic and real image sets are  
 349 shown in the following sections.

### 350 3.3. Determining Shutter Angle

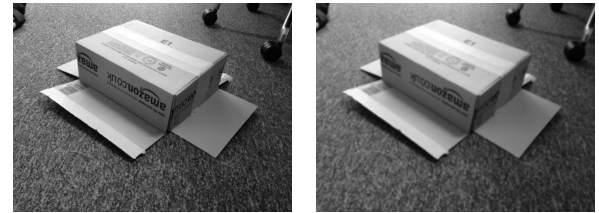
351 By combining the results for rotation obtained from a  
 352 single frame, and those from a pair of frames - it should  
 353 be possible to calculate the exposure time of the frame as  
 354 a fraction of the framerate, simply by dividing the motion  
 355 magnitude obtained from blur by that of the frame-to-  
 356 frame track. This calculation could further be simplified  
 357 by using just the geometric distance between points identi-  
 358 fied by searching along the radial or circular profiles. How-  
 359 ever, it is envisaged that by performing the extra stages  
 360 of rotation estimation will provide a more robust estima-  
 361 tion for shutter angle. This is because both methods for  
 362 determining rotation include the rejection of outliers as an  
 363 important stage in the calculation of the magnitude.

### 364 3.4. Determining Amount of Blur in an Image

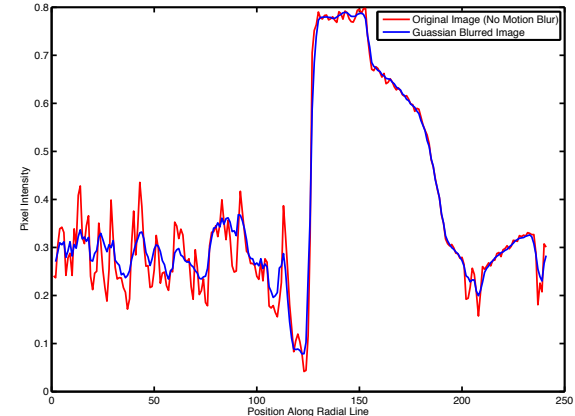
365 It is envisaged that the methods presented previously  
 366 will only work well if there is a sufficient amount of blur  
 367 from motion present in the image. This is a limitation also  
 368 highlighted by the authors of [6]. In order to evaluate the  
 369 effectiveness of the method for accurately determining the  
 370 scale change of different magnitudes across different sets of  
 371 images, we propose a method for quantifying the amount  
 372 of blur present across the whole image. Furthermore, it  
 373 is proposed that this accuracy measure could be used to  
 374 correct estimates over further footage of the same scene,  
 375 given a ground truth for some initial data. This could  
 376 be useful in such a situation where, for example, exter-  
 377 nal hardware was being used to record the change in lens

378 barrel and hence focal length position - and this hardware  
 379 becomes unsynchronised or uncalibrated throughout the  
 380 shot. Such situations are not uncommon and can require  
 381 a large amount of work post-production to rectify. We  
 382 would also typically expect the methods described here to  
 383 be applied on a sequence of frames, some of which will not  
 384 contain any change in focal length or rotation. As part  
 385 of the process for estimating shutter angle from rotation  
 386 (a change in an extrinsic parameter), it is possible to ac-  
 387 curately deduce cases for which rotation and hence blur  
 388 is zero using the optical flow method (results of which are  
 389 shown by Fig. 8) which must be performed on each pair of  
 390 frames. As previously stated, it is not possible to identify  
 391 an blurred edge of length zero, so in the case of zero focal  
 392 length change - the proposed algorithm will always return  
 393 a result greater than zero. Classifying the blur character-  
 394 istics of a frame with zero scale change would therefore  
 395 allow for automatic identification of these frames

396 In the case of focal length from a single frame the fol-  
 397 lowing method is used to determine the amount of blur  
 398 present in an image. We define blur energy ratio  $r_{\text{blur}}$  in  
 399 an image as the average ratio between the energy of a pro-  
 400 file of pixel intensities along a set of radial lines across an  
 401 image, and the average energy of the same set of sample  
 402 lines of the same image after having undergone a gaussian  
 403 blur operation. In this work we used a Gaussian kernel  
 404  $\omega = [\frac{1}{4} - \frac{a}{2}, \frac{1}{4}, a, \frac{1}{4}, \frac{1}{4} - \frac{a}{2}]$  where  $a = 0.375$ , and in order  
 405 to produce a more significant result for the difference in  
 406 energies across a radial profile, the difference between the  
 407 top and the 3rd level of the Gaussian reduction pyramid  
 408 is sampled. Similarly to the method used for determining  
 409 scale change from motion blur, radial lines are sampled  
 410 from the outside edges of the image inward - initialised at  
 411 10 pixel intervals along the edges of the image. The rea-  
 412 soning behind this is that an image that contains motion  
 413 blur will have a lower energy (lower frequency of changes in  
 414 intensity) than a sharp, non-motion blurred image - as de-  
 415 scribed in earlier sections. However the ratio of energy be-  
 416 tween this motion blurred image and its gaussian blurred  
 417 equivalent should be larger than the ratio of profile en-  
 418 ergy between a non motion-blurred image and its blurred  
 419 equivalent. This is illustrated in Figure 6 and Figure 7,  
 420 where it can be seen that for a non-motion blurred orig-  
 421 inal image, there is a much higher frequency (and hence  
 422 greater energy) of intensity change for the original image  
 423 than the gaussian-blurred equivalent image. For the pro-  
 424 files shown in Figure 7, the frequency of changes in inten-  
 425 sity for the original image is much closer to that of the  
 426 Gaussian-blurred equivalent. We define energy as the sum  
 427 of squared values of image intensity along the profile line,  
 428 and sample along multiple profile lines, taking the mean  
 429 ratio of energies across all lines over the image pair to be  
 430 value for the difference in image energy.

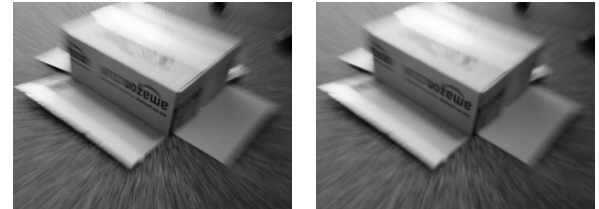


Original Image with No Motion Blur (Sharp image)  
 Gaussian Blur of Sharp Image

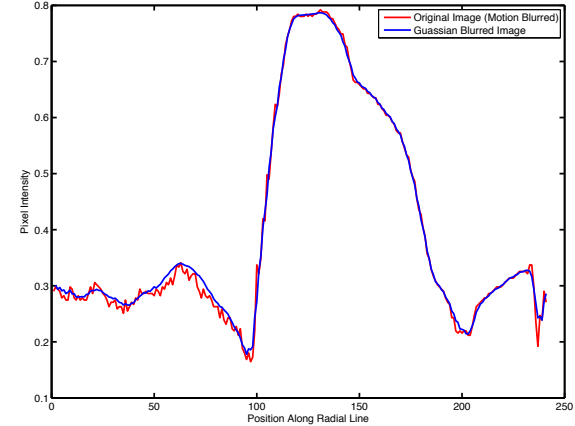


Pixel Intensity Profiles for Non-Motion Blurred Image and Corresponding Gaussian Image

Figure 6: Non-Blurred image and Gaussian Blurred Image with Corresponding Profile Lines



Original Image with Motion Blur  
 Gaussian Blur of Motion Blurred Image



Pixel Intensity Profiles for Motion Blurred Image and Corresponding Gaussian Image

Figure 7: Motion-Blurred image and Gaussian Blurred Image with Corresponding Profile Lines

431 **4. Results**

432 Presented in this section are the results obtained from a  
433 variety of tests, both on synthetic and real footage. In the  
434 case of synthetic images, a single static photograph had an  
435 animated scale change applied using the Nuke compositing  
436 tool (a 2D image manipulation package well suited to ap-  
437 plying transforms, filters and animation and used widely  
438 in the post production industry). Motion blur for this  
439 set of images was then simulated for the specified shutter  
440 opening time at each frame.

441 Initially results are shown as in [1] for the raw out-  
442 put produced from running the algorithms for estimating  
443 changes in intrinsic values on a sequence of frames without  
444 first considering the amount of blur present in each frame  
445 of the sequence using the method described in Sec. 3.4.

446 For real image sequences, an external electro-mechanical  
447 *zoom encoder* was attached to the lens on the camera used  
448 to capture the footage. This is a proprietary device that  
449 uses a geared rotary encoder meshed with the zoom ring  
450 on the lens barrel to track change in rotational position  
451 of the ring. After a simple calibration and synchronisa-  
452 tion, this data can be used to infer the focal length at a  
453 particular frame, independently from the image captured  
454 by the camera. Such devices are commonly used through-  
455 out the visual effects and post-production process as they  
456 provide a reliable method of measuring changes in camera  
457 parameters.

458 For the production of ground-truth values for camera  
459 rotation, the camera was rigidly attached to a high-end  
460 rate-gyro capable of determining rotation up to a speed  
461  $175^\circ/\text{sec}$  with a standard error of  $0.0005^\circ/\text{sec}/\sqrt{\text{Hz}}$ . [12]  
462 presents a comprehensive description of the specifications  
463 and sources of error in inertial measurement systems.

464 The values obtained from both the ground truth and  
465 original estimates of a real data-set for change in focal  
466 length are then used to calculate the expected error factor  
467 for each range of blur magnitude present in the frame. The  
468 ground truth magnitude for scale change is also used to  
469 validate that our measurement of blur present in a frame  
470 is effective. These error metrics are then used to attempt  
471 to produce a more accurate estimate of scale change from  
472 blur, using new footage of the same scene.

473 **4.1. Synthetic Tests**

474 To test the algorithms against a synthetic and known  
475 ground truth for a change in focal length, shutter angle,  
476 and rotation, the Nuke compositing tool was used to create  
477 an animated series of frames from a single image.

478 **4.1.1. Focal length change from a Single Frame**

479 Results for the motion estimates for a set of rotation  
480 changes and changes in focal length are shown here. In  
481 both cases, as it is not possible to determine the direction  
482 of motion from a single frame, all of the values for both  
483 focal length change and rotation are absolute values. Fig.  
484 10 shows a plot for results obtained for determining the

485 change in scale induced by a change in focal length. In  
486 panel (i), the dashed blue and red lines should ideally be  
487 identical, and in the scatter chart in panel (ii), the points  
488 should lie in an  $x = y$  line. In this result, the chart in  
489 panel (i) also shows the change in scale corrected for the  
490 known shutter exposure time of the virtual camera, which  
491 should equal the frame to frame estimate of scale (the true  
492 scale in this case). For most frames, it can be seen that  
493 the raw estimation from blur overestimates the true scale  
494 value. This is to be expected, as if there is zero blur, the  
495 sharpest edge in the blur profile to be found (as described  
496 in Sec. 3) will still be at least one pixel (in practice on real  
497 photographs, this will likely be more) - which will there-  
498 fore always result in some scale change being estimated.  
499 This is the effect that we aim to compensate for using the  
500 blur-information obtained using the method described in  
501 Sec. 3.4 to estimate the expected error of results of a scene,  
502 and the results for this when applied to a real scene are  
503 shown in Sec. 4.3.

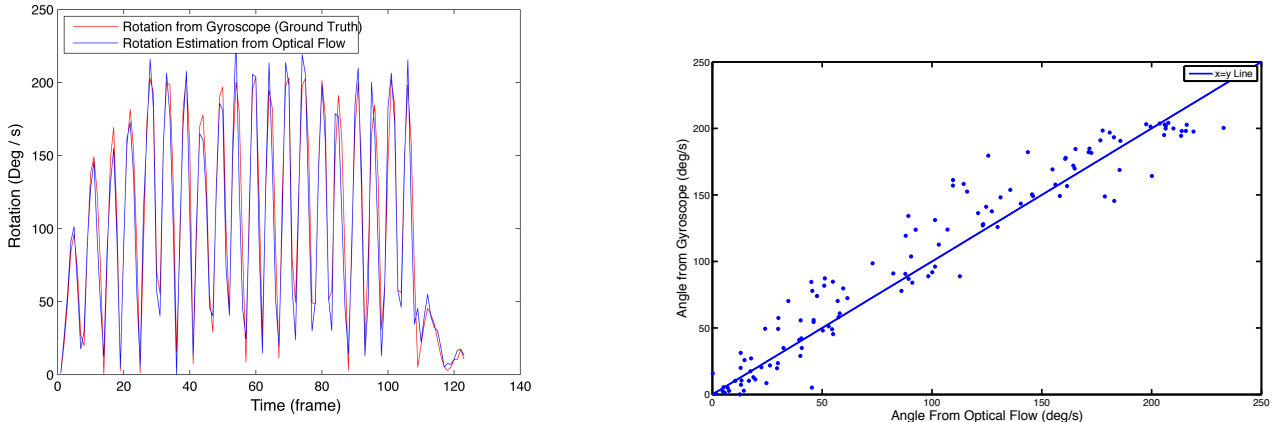
504 **4.1.2. Shutter Angle and Rotation Estimation from a pair  
505 of Frames**

506 Figure 9 shows results from a synthetic sequence under-  
507 going a series of varying rotations and with an animated  
508 shutter angle. Panel 1 in this figure shows the estimates  
509 for the magnitude of motion blur obtained from both the  
510 pair of frame method and single frame Klein and Drum-  
511 mond method, the latter being un-corrected for the known  
512 shutter exposure time. From this result it can be seen  
513 that in many cases where there is only a small amount of  
514 rotation, the single frame method from motion blur will  
515 over-estimate the amount of rotation that has occurred.  
516 However, the blur based system appears to consistently  
517 underestimate the value for rotation when there is a sig-  
518 nificant change in rotation, and this behaviour is to be  
519 expected - as detailed in Sec. 3.1, as the motion from blur  
520 will only represent a fraction of the frame time, whereas  
521 the frame to frame track will represent the full movement  
522 between frames.

523 Due to the noise in measuring rotation from blur, the  
524 resulting estimate for shutter angle is smoothed using a  
525 moving average filter (with a span of 4 frames) across the  
526 frame-set. This filtering is necessary because whilst the  
527 RANSAC algorithm described in Sec. 3.1 is able to reduce  
528 the effect of outlying estimates for rotation of the frame,  
529 certain conditions (further described in Sec. 5) will always  
530 produce incorrect results. The most significant source of  
531 error occurs when the magnitude of blur in the image is  
532 not sufficient for the accurate detection of the true change  
533 in focal length or rotation. By filtering these estimates we  
534 are able to reduce the impact of these errors whilst still  
535 maintaining an acceptable level of accuracy over periods  
536 where there is only a small amount of rotation present in  
537 the frame. A moving average filter was selected as this  
538 is a simple to implement filter that will filter out high-  
539 frequency changes in the estimate for shutter angle. We do  
540 not expect the shutter angle to change at every frame, so



Rotation with Gyroscope to Validate Rotation from Optical Flow Calculation (Poster)



Comparison of Rotation from Optical Flow Calculation with Gyroscope Data (Ground Truth) - Performed on the 'Poster' Real Dataset This dataset was produced with a rigid camera-gyroscope rig in order to validate that the estimates produced by the optical flow algorithm for rotation in the presence of motion-blur were accurate when the rotation magnitude and axis of the camera is arbitrary and otherwise unknown.

Figure 8: Comparison of Results from Optical Flow based Rotation Estimation and Gyroscope Readings

this method allows for a single step change in shutter angle to be easily identified, whilst filtering the noisy calculation. Furthermore, outlying estimates that predict the shutter angle to be 1 or greater (i.e. the shutter was open longer than the frame time) are also automatically discarded.

#### 4.2. Real Footage

The algorithms described in this work were tested over a set of real images captured by a Canon 700D SLR Camera era along with a 70-200mm lens. The scenes shot were indoors and in good lighting conditions, and outdoors with natural light and some movement of objects in the scene (for example, trees moving in the wind and pedestrians walking through the frame). For the case of focal length estimation, a rotary encoder was attached to the lens barrel to track changes in rotation of the zoom wheel, and hence changes in the focal length. Each sequence consists of approximately 300 frames. In the case of rotation - the camera was rotated quickly and manually around an axis at various speeds and magnitudes, in order to produce a sequence that would exhibit large amounts of motion blur. Likewise, for changes in focal length, the zoom was also changed quickly and at varying speeds and magnitudes whilst filming. In all cases, the shutter speed was set to a constant 1/30th of a second - apart from the Chairs dataset where it was changed to 1/60th of a second after approximately 160 frames.

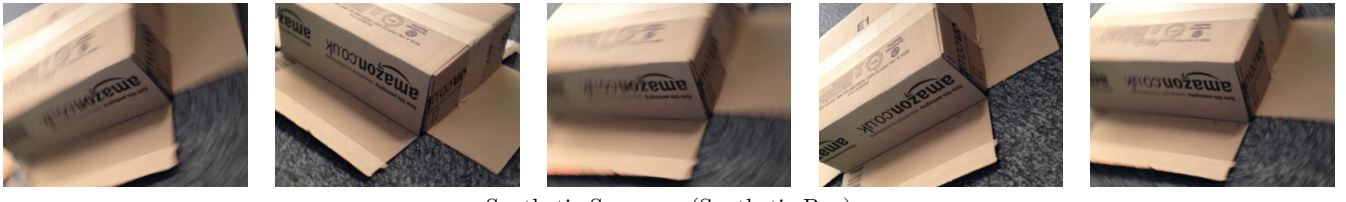
##### 4.2.1. Shutter Angle and Rotation Estimation from a Pair of Frames

In order to validate the results produced using the 2 frame optical flow based method for determining camera rotation, the estimates obtained using this method on real footage were compared with the results obtained from a gyroscope rigidly attached to the camera during rotations around an axis. Figure 8 shows the results of this test. Ideally, the line plot for the angle estimated from optical flow against the gyroscope data should be identical, and the scatter plot for this data tend to an  $x = y$  line.

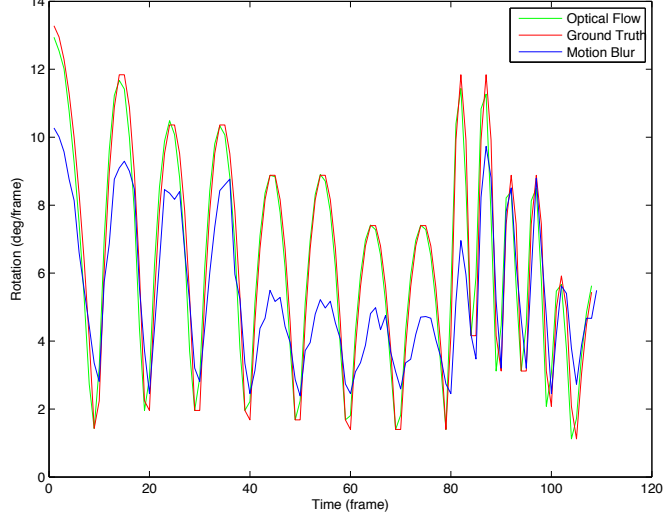
Shown in figure 9 are the results obtained from rotating a camera around an axis over various magnitudes, and estimating rotation from both optical flow and blur. During shooting, the camera's shutter speed was changed from 1/30th of a second (0.83 of a frame at 25fps) to 1/60th of a second (0.415 of a frame at 25fps). Figure 9 also shows the estimated shutter angle as a fraction of the frame from the difference in estimations. As with the results from synthetic sequences, the value for shutter angle was calculated from a smoothed estimate for rotation from blur at each location above a threshold value.

##### 4.2.2. Focal Length Change

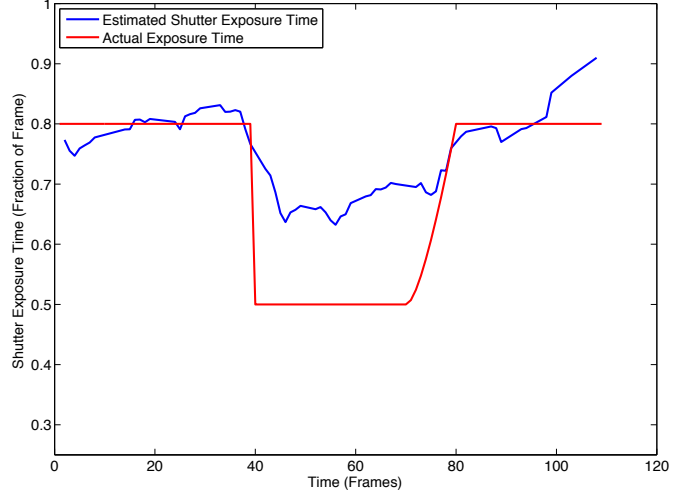
Presented in figure 11 are the results for determining a change in focal length using a single frame using the method described previously. As with rotation from blur, the single frame method of determining focal length change



Synthetic Sequence (Synthetic Box)



(i)

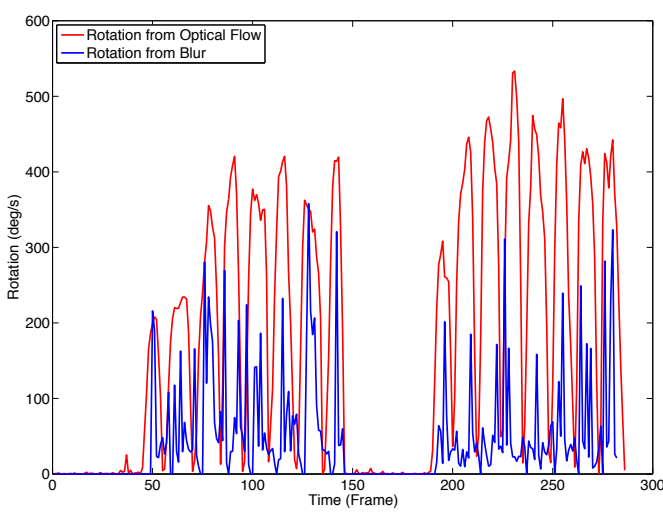


(ii)

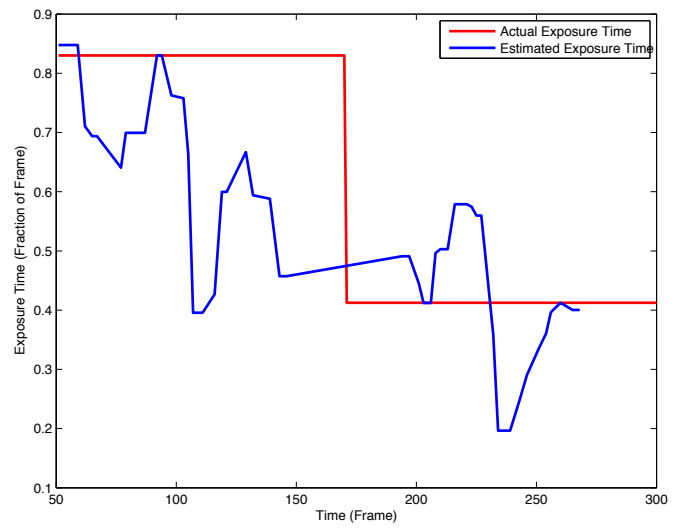
Shutter Angle and Rotation Estimates from a Synthetic Dataset (Synthetic Box Sequence)



Rotation with Changing Shutter Angle. The final two frames above have a shutter angle of half the first three. (Chairs)



(iii)



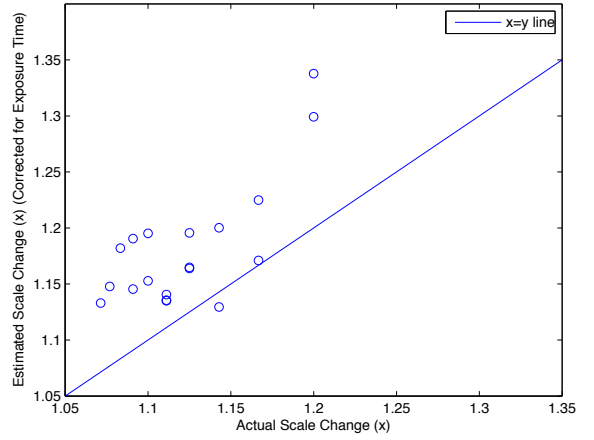
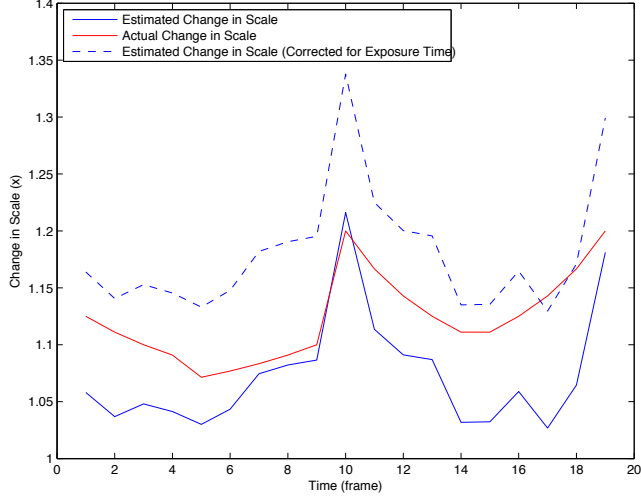
(iv)

Shutter Angle and Rotation Estimates from a Real Dataset ('Chairs' Sequence)

Figure 9: Results for Estimating Rotation and Shutter Angle from Blur and Optical Flow



Synthetic Focal Length Change (Zoom Synthetic Boxes)

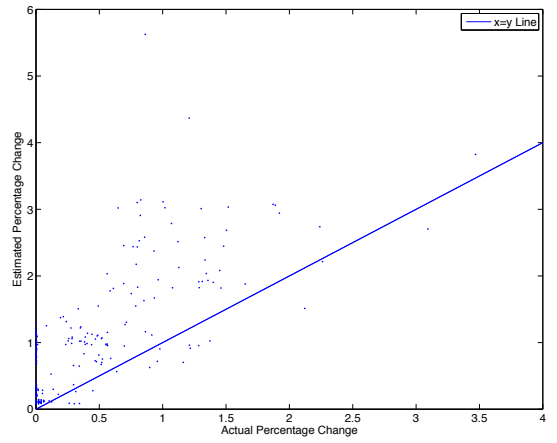
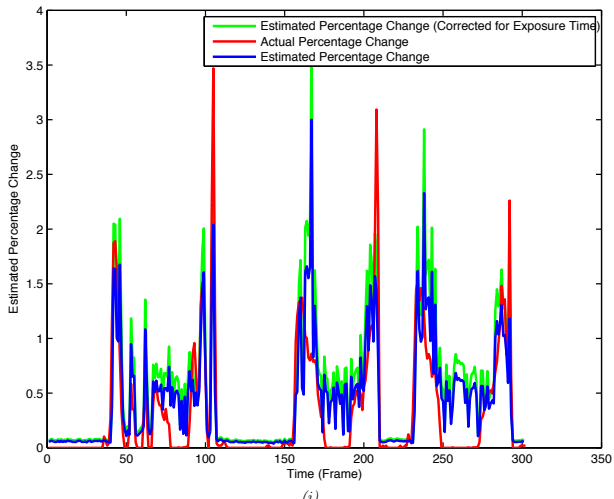


Change in Focal Length Estimates from a Synthetic Dataset. Ideally, the dashed-blue and solid-red lines in the left-hand chart should align, and the scatter plot should tend to an  $x = y$  line.

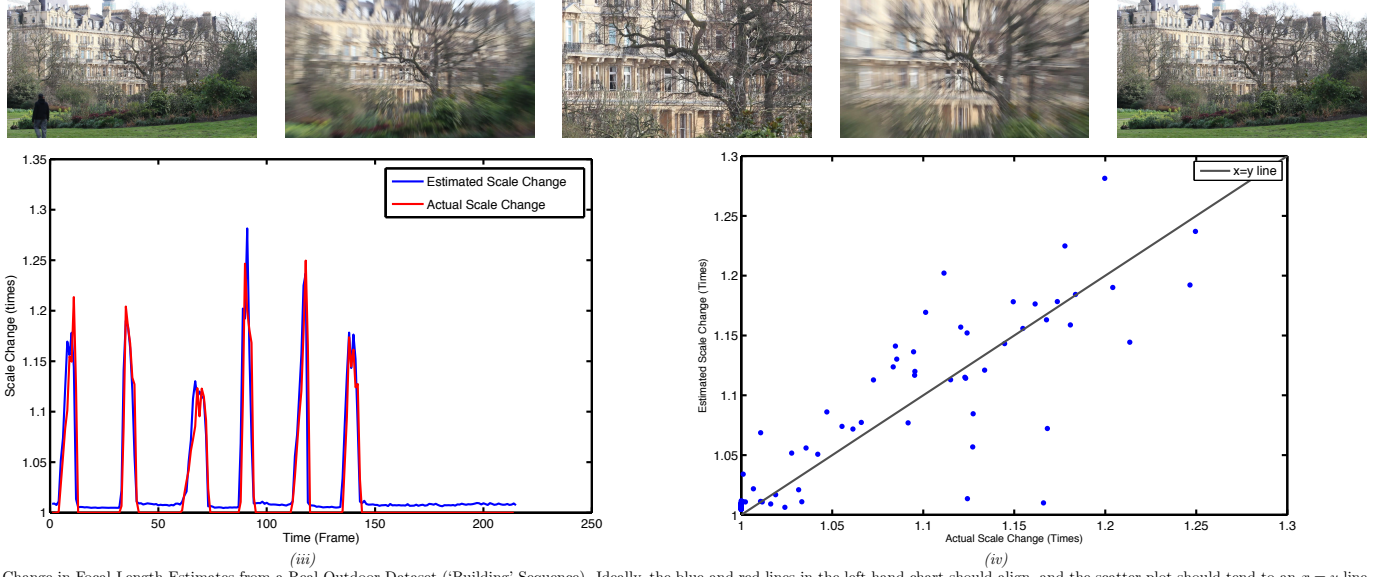
Figure 10: Results for Estimating Change in Focal Length from Blur with a Synthetic Data Set



Real Focal Length Change (Zoom Boxes)

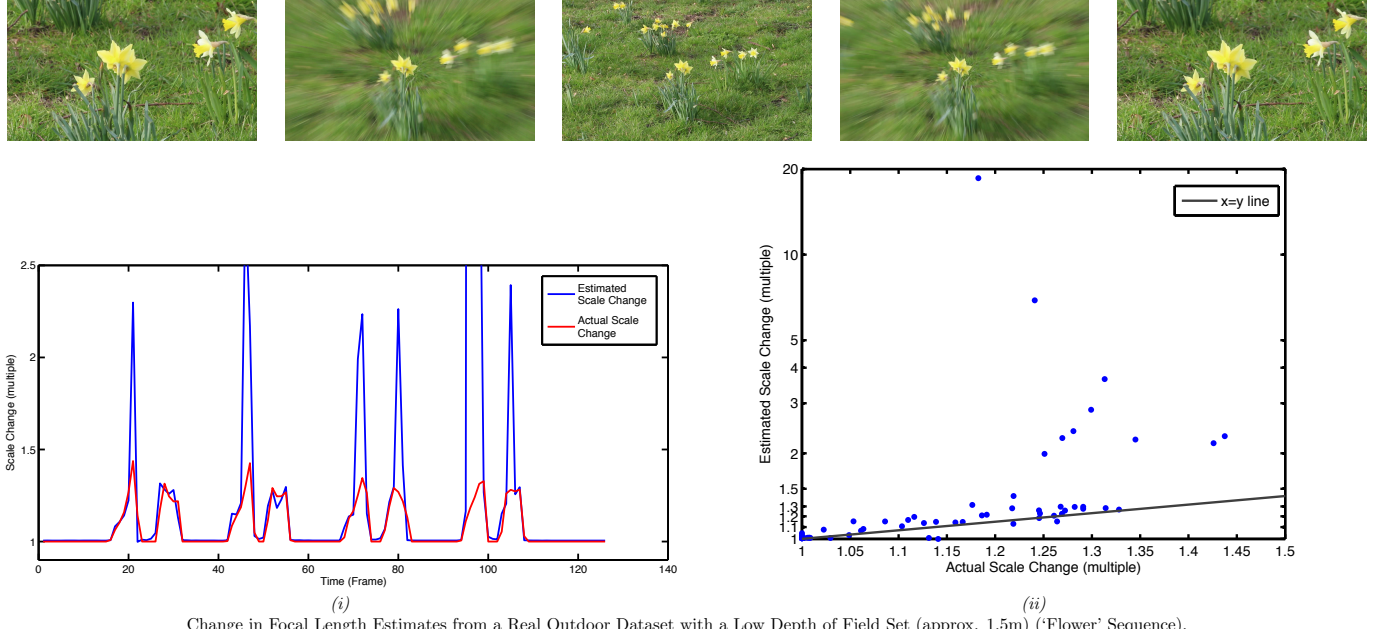


Change in Focal Length Estimates from a Real Dataset ('Zoom Boxes' Sequence). Ideally, the green and red lines in the left-hand chart should align, and the scatter plot should tend to an  $x = y$  line.



Change in Focal Length Estimates from a Real Outdoor Dataset ('Building' Sequence). Ideally, the blue and red lines in the left-hand chart should align, and the scatter plot should tend to an  $x = y$  line.

Figure 11: Results for Estimating Change in Focal Length from Blur for Real Datasets



Change in Focal Length Estimates from a Real Outdoor Dataset with a Low Depth of Field Set (approx. 1.5m) ('Flower' Sequence). Ideally, the green and red lines in the left-hand chart should align, and the scatter plot should tend to an  $x = y$  line.

Figure 12: Results for Estimating Change in Focal Length from Blur on a scene with a low Depth of Field

594 is unable to determine the direction of the change, hence  
 595 data from the zoom encoder (taken as the ground truth)  
 596 is converted to an absolute change in value. The initial  
 597 indoor footage - ‘Zoom Boxes’ sequence in Fig. 11 panels  
 598 (i) and (ii) was shot with good lighting conditions, how-  
 599 ever it can be seen that there is a smaller amount visual  
 600 texture in the image, such as sharp edges and high con-  
 601 trast, when compared to the outdoor ‘Building’ sequence  
 602 (panels (iii) and (iv) of the same figure). The result set for  
 603 the ‘Building’ sequence as shown in panels (iii) and (iv) of  
 604 Fig. 11 are clearly of a higher quality, and would suggest  
 605 that the presence of good visual texture and a large num-  
 606 ber of sharp edges in the scene is important for achieving  
 607 accurate results.

#### 608 4.2.3. Alignment of Sensor Data with Video Footage

609 During capture of real data using both the gyroscope  
 610 and zoom encoder equipment, it was necessary to syn-  
 611 chronise the recording equipment with the video frames.  
 612 This is performed by showing the camera a ‘digislate’ - a  
 613 device which displays a time-code which refreshes at the  
 614 specified framerate at the start of recording, and synchro-  
 615 nising electronically this time-code with the data record-  
 616 ing equipment. When the video is retrieved, the frames  
 617 are manually inspected to read the time-code displayed on  
 618 the device and correlate with the frame number of the se-  
 619 quence. Whilst this is a straightforward process to perform  
 620 in a controlled environment, it is not practical in every  
 621 shooting environment, e.g. if shooting from an aircraft. In  
 622 such cases, manually aligning the data to the frame can  
 623 be a difficult process. If an estimate can be found from  
 624 frames with motion blur present as to the change in ei-  
 625 ther zoom or rotation, then it could be used to assist in  
 626 the alignment of the data in the case of failed synchroni-  
 627 sation. One such way of achieving this would be the use  
 628 of cross-correlation over both signals (estimate from blur  
 629 and ground truth from sensors). Shown in figure 13 are the  
 630 results from using the method of focal length estimation  
 631 described in this work to align data from the zoom encoder  
 632 sensor, compared to the actual synchronised values. In this  
 633 case, the zoom encoder started recording positions before  
 634 the camera started recording frames (recording changes in  
 635 zoom that were not filmed) - shown in panel (i) of Fig. 13  
 636 and continued recording after the camera was stopped.  
 637 The algorithm for estimating the amount of blur was run  
 638 on the captured footage the results of which are shown in  
 639 panel (ii) of the same figure and the data aligned using  
 640 the results from the algorithm and cross correlation with  
 641 the unsynchronised stream of data, the predicted align-  
 642 ment shown in panel (iii). This predicted synchronisation  
 643 shift differs by 1 frame from the actual known value of 908  
 644 frames.

#### 645 4.3. Evaluating Algorithm Efficacy vs. Amount of Blur 646 Present

647 Section 3.4 describes the method used for determining  
 648 the amount of blur present in a scene, and shown here are

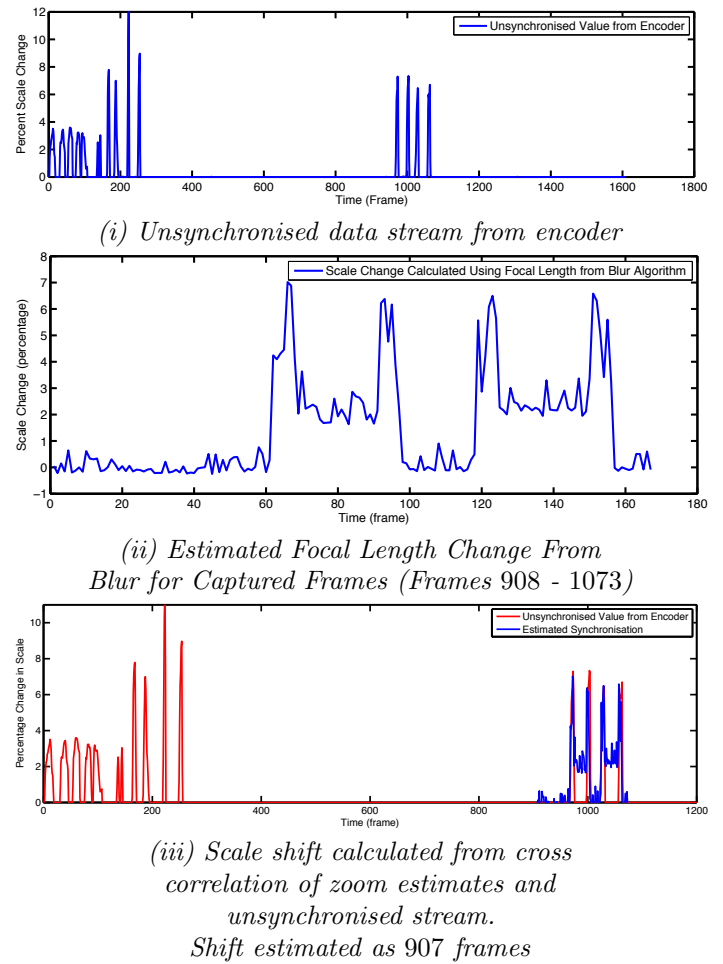


Figure 13: Results for Estimating the Synchronisation between Camera and Zoom Encoder

the results for determining this metric ( $r_{\text{blur}}$ ) along with the accuracy of the zoom estimates from Sec. 4.2.2. In order to evaluate the amount of blur necessary in an image to produce an accurate result, we calculate the amount of blur present in each frame of the sequence of real images using the method described in Sec. 3.4, where each frame has undergone a change in focal length of varying magnitude (including zero). This magnitude of blur is then compared to error between the estimate of scale change and the ground truth values for scale change at that frame. Figures 14,15 and 16 show the results of this analysis for each of the real datasets presented in Sec. 4. We would expect to see a higher proportion of over-estimates for the magnitude of scale change in the image, particularly at a low known scale change. The graphs for this analysis tend to support this conclusion - however, in all three cases there appears to be a reasonable amount of error when the scale change is greater than zero - but the amount of blur present in the image is not at its maximum. In the graphs of figures 14,15 and 16, this can be seen as a reported under-estimate towards the middle of the blur-ratio scale (the  $x$  axis) where the red true scale-change line rises. This result would further support the conclusion that as a condition of a scale change being accurately estimated, it must cause significant motion blur in the image. However, it would appear that at the higher end of the scale change the method clearly over-estimates the true scale change by a considerable amount, and can sometimes under-report it. This would appear to contradict the theory that larger scale changes, resulting in larger amounts of blur present in the image (reflected by the rise of  $r_{\text{blur}}$ ) should result in more accurate predictions using this method.

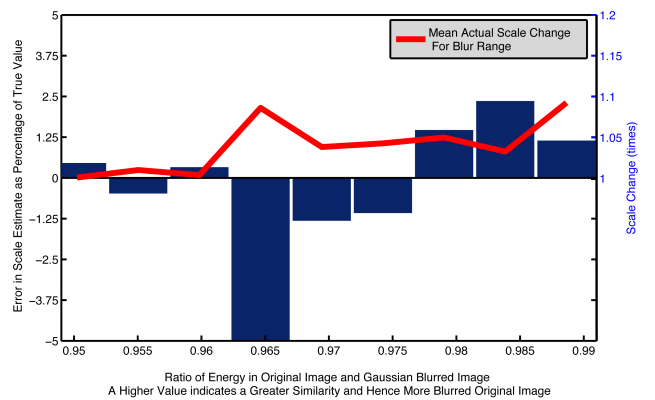


Figure 14: Results for comparing amount of blur in a frame with scale change estimate accuracy for the ‘Boxes’ Dataset

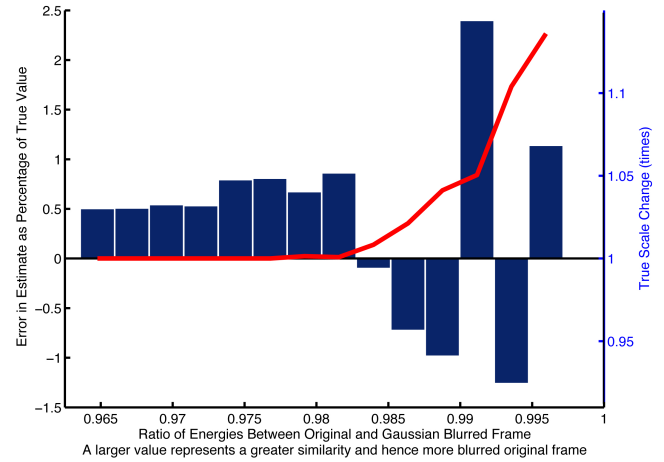


Figure 15: Results for comparing amount of blur in a frame with scale change estimate accuracy for the ‘Building’ Dataset

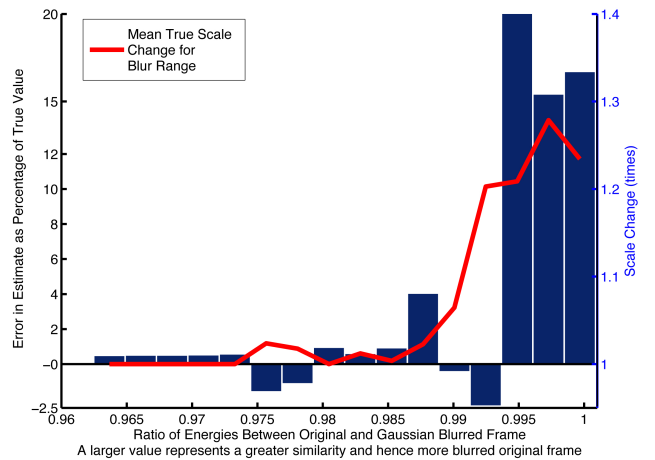


Figure 16: Results for comparing amount of blur in a frame with scale change estimate accuracy for the ‘Flower’ Dataset

Using these results, it is proposed that a ‘confidence’ value of the estimated result can be predicted, in that for a images with a range of values calculated for  $r_{\text{blur}}$ , the

expected result from using the original method for scale change from blur would be accurate to within a certain percentage error. This value could then be used to increase the accuracy of further results obtained from the same scene, in a situation where a ground truth would not be available. This would be especially useful in order to be able to categorise frames in which the scale change is likely to be zero, and hence saving the need to attempt to calculate a transform estimate for this frame. Applying the error metrics determined for the ‘Building’ scene to further footage of this scene (with the camera at a slightly different orientation) produces the results shown in Fig. 17 and Fig.18. These results are obtained by calculating the blur ratio ( $r_{\text{blur}}$ ) from each frame and producing a ‘corrected’ result for this frame by applying the error metric for the range in which  $r_{\text{blur}}$  for this frame sits to the initial estimate. That is, if the frame is judged to have a value for  $r_{\text{blur}}$  as 0.987, the corrected result will be the estimated result scaled up by the error for this blur ratio from Fig. 15. If a value for  $r_{\text{blur}}$  is encountered that is not present within Fig. 15, then the value for scale change produced by the original algorithm is used. Similarly, if the value for  $r_{\text{blur}}$  is below a threshold indicating that no scale change is taking place, the corrected value is clamped to 0. We find that the cross correlation coefficient between the naive, raw estimates and the actual values to be 0.865, whereas the correlation coefficient between the corrected set and true values to be slightly better at 0.879.

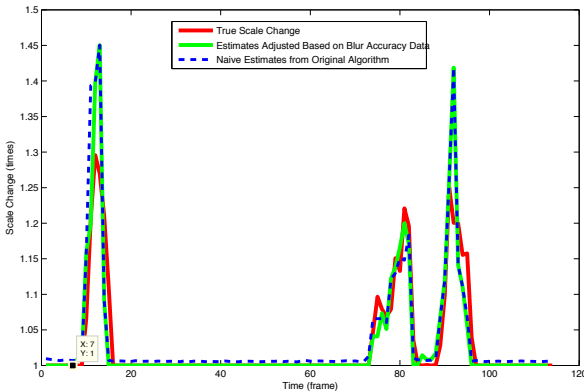


Figure 17: Comparison between the ‘Naive’ Focal Length from Blur Algorithm, and the ‘Blur Aware’ Method that multiplies results from the Naive Method with Error Factors Determined in Section 4.3. Ideally, the green line should be identical to the red, and closer to this than the blue line. Frames that are determined to have no scale change (a blur-ratio of less than 0.981) are capped at zero.

#### 4.4. Effects of Depth of Field

Figure 12 shows the result of a real scene with a low depth of field (the ‘Flower’ dataset). The focal distance in this scene was set to approximately 1.5m, whereas in the other real scenes used in this work, the focal distance is set to infinity. It can immediately be seen in panels (i)

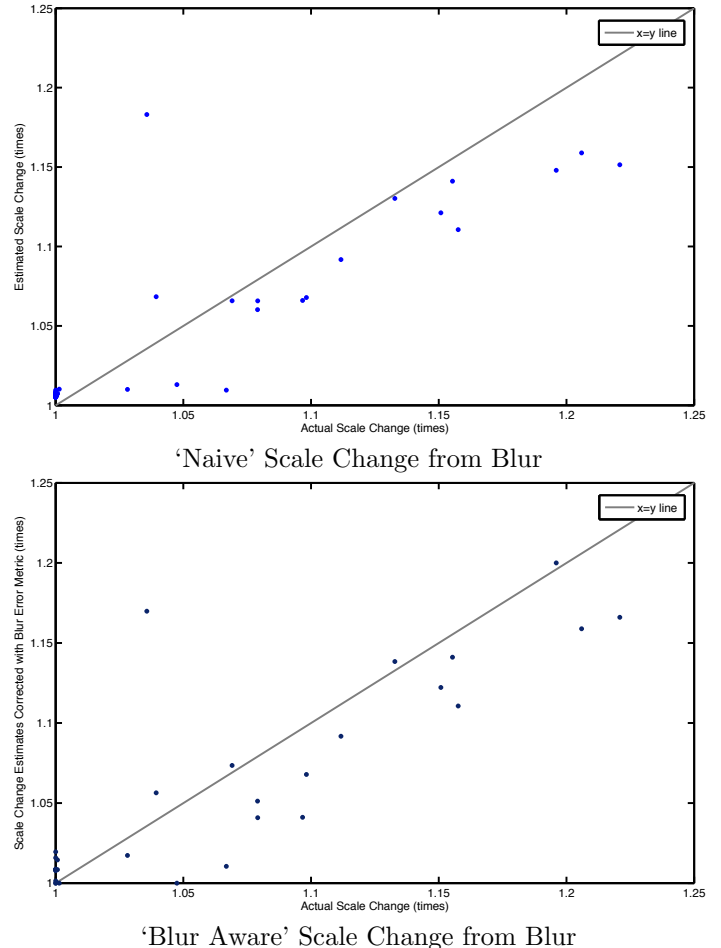


Figure 18: Comparison between the ‘Naive’ Focal Length from Blur Algorithm, and the ‘Blur Aware’ Method. Ideally, the points should tend to an  $x=y$  line, and the blur aware method should have points closer to this than the ‘naive’ method

and (ii) that the results are somewhat more inaccurate than those from other images, with a tendency to greatly overestimate the true extent of scale change during large changes in scale. Images with a low depth-of field would typically have more blur in the frame regardless of motion blur introduced by scale change during shutter opening. This is something that Fig. 16 would confirm - as the zero, or close to zero scale change extends further along the blur ratio scale than in the results shown for other sequences. In theory, as long as part of the image is in focus, and this part has enough visual texture - such as sharp lines, then these would be blurred by the scale change and not from defocus - and could be used to calculate the scale change. In practice however, it is often the case that the in-focus part of the image would be at the centre of the image. As discussed in Sec.3.1, it is likely that points towards the centre of the image will be minimally scaled - and therefore unlikely to give a reliable estimate for the focal length change.

737 

## 5. Limitations

738 The results obtained from using motion blur in this  
 739 work do suffer from several of the limitations discussed in  
 740 the original Klein & Drummond paper. Notably, one of  
 741 the most significant problems encountered for the estima-  
 742 tion of parameters using blur is the need for a reasonable  
 743 amount of blur to be present in order to be successfully  
 744 detected. We have however presented a viable method to  
 745 overcome this limitation somewhat by using prior knowl-  
 746 edge of the error of the scale change estimate for a scene,  
 747 and the amount of blur present in an image in order to  
 748 better predict the scale change.

749 Another significant issue with the use of a single motion-  
 750 blurred frame to estimate parameters is the inability of the  
 751 system to cope with frames that have undergone more than  
 752 one transformation - e.g. a rotation alongside a change in  
 753 focal length. Another significant limitation of this work is  
 754 the inability of the system to cope with large movement  
 755 of objects in the scene. Our results suggest that a small  
 756 amount of movement, such as pedestrians in a scene or a  
 757 tree blowing in the wind will still allow for accurate results  
 758 to be obtained. However, experimentation has shown that  
 759 if the scene is completely obscured by movement, such as a  
 760 vehicle passing in front of the camera during a focal length  
 761 change, will cause the algorithm to fail.

762 Other limitations described in [6] for estimating pa-  
 763 rameters from blur are also present in this system, such as  
 764 the intolerance to strobing, over-saturation, the require-  
 765 ment for pure rotation and a constant centre of rotation.  
 766 However, when combined with the optical flow method de-  
 767 scribed in [17], it is possible to determine the ‘sign’ of the  
 768 rotation estimates. The method presented in [17], whilst  
 769 extremely accurate (as shown by fig. 8), does have a signif-  
 770 icant limitation of requiring a large amount of resources to  
 771 compute - often necessitating frames to be re-scaled prior  
 772 to calculation. On average, for each blurred pair of frames  
 773 at a size of  $640 \times 480$  pixels, it would take approximately  
 774 30 seconds to compute an estimate for the optical flow,  
 775 whereas the methods from blur would compute a result in  
 776 near real-time on the same hardware ( $\approx 30$  m/s), although  
 777 this speed is highly dependent on the number of edgel sites  
 778 selected and also the size of the image. Recent works in  
 779 [2] and [3] have attempted to address this limitation.

780 Another factor that may have an effect on the result  
 781 obtained for real footage would be the differences in blur  
 782 introduced into a frame by a camera’s rolling shutter (de-  
 783 tailed in [8]). All of the algorithms described and used  
 784 in this paper operate under the assumption that when  
 785 a frame is blurred due to motion, the blur is always as-  
 786 sumed to be constant across this frame. In a camera with  
 787 a rolling shutter, each line of the sensor in the camera is  
 788 sampled sequentially at different times. Therefore, during  
 789 fast movement, in a camera with a rolling shutter, this  
 790 assumption that all parts of the image will be blurred by  
 791 a constant amount cannot be true. Investigating the im-  
 792 pact and ways of minimising these effects in the algorithms

793 using blur would be an important next stage of research.

794 

## 6. Conclusions

795 This paper has shown an earlier method for determin-  
 796 ing changes in focal length during a single motion blurred  
 797 frame, and has produced promising results from this method  
 798 that allows for the estimates to be calculated quickly. We  
 799 have also extended and combined two previous works in  
 800 order to estimate the shutter angle of a frame. We have  
 801 extended upon this work by presenting a new method to  
 802 work with the original as part of an extended system in  
 803 order to address previous limitations and enhance the ac-  
 804 curacy of this new algorithm. We have also tested our  
 805 methods on a new real data set and have been able to  
 806 demonstrate that this improved method gives more accu-  
 807 rate results, furthermore, we have examined how this  
 808 system might cope with an image sequence with a shallow  
 809 depth of field - and have uncovered potential limitations  
 810 that this may present. An area of further research would  
 811 be extending this system to handle frames which have been  
 812 blurred by more than one type of motion - such as in the  
 813 case of a translation and rotation, and work into this topic  
 814 is ongoing.

- 815 [1] Alastair Barber, Matthew Brown, Paul Hogbin, and Darren  
 816 Cosker. Estimating camera intrinsics from motion blur. In  
 817 *Proceedings of the 11th European Conference on Visual Media*  
 818 *Production, CVMP ’14*, pages 6:1–6:10, New York, NY, USA,  
 819 2014. ACM.
- 820 [2] Xiaogang Chen, Jie Yang, Qiang Wu, Jiajia Zhao, and Xi-  
 821 angjian He. Directional high-pass filter for blurry image analy-  
 822 sis. *Signal Processing: Image Communication*, 27(7):760 – 771,  
 823 2012.
- 824 [3] Sunghyun Cho and Seungyong Lee. Fast motion deblurring.  
 825 In *ACM SIGGRAPH Asia 2009 Papers, SIGGRAPH Asia ’09*,  
 826 pages 145:1–145:8, New York, NY, USA, 2009. ACM.
- 827 [4] Karen Goulekas. *The VES Handbook of Visual Effects*, chapter  
 828 Postvis, pages 62–66. Elsevier, 2010.
- 829 [5] Alexandre Karpenko, David Jacobs, Jongmin Baek, and Marc  
 830 Levoy. Digital video stabilization and rolling shutter correction  
 831 using gyroscopes.
- 832 [6] Georg Klein and Tom Drummond. A single-frame visual  
 833 gyroscope. In *Proc. British Machine Vision Conference*  
 834 (*BMVC’05*), volume 2, pages 529–538, Oxford, September 2005.  
 835 BMVA.
- 836 [7] Wenbin Li, Yang Chen, JeeHang Lee, Gang Ren, and Darren  
 837 Cosker. Robust optical flow estimation for continuous blurred  
 838 scenes using rgb-motion imaging and directional filtering. In  
 839 *IEEE Winter Conference on Applications of Computer Vision*  
 840 (*WACV*), 2014.
- 841 [8] Chia-Kai Liang, Li-Wen Chang, and H.H. Chen. Analysis and  
 842 compensation of rolling shutter effect. *Image Processing, IEEE*  
 843 *Transactions on*, 17(8):1323–1330, Aug 2008.
- 844 [9] Huei-Yung Lin. Vehicle speed detection and identification from  
 845 a single motion blurred image. In *Application of Computer*  
 846 *Vision, 2005. WACV/MOTIONS ’05 Volume 1. Seventh IEEE*  
 847 *Workshops on*, volume 1, pages 461–467, Jan 2005.
- 848 [10] S.K. Nayar and M. Ben-Ezra. Motion-based motion deblurring.  
 849 *Pattern Analysis and Machine Intelligence, IEEE Transactions*  
 850 *on*, 26(6):689–698, June 2004.
- 851 [11] T. Okatani and K. Deguchi. Robust estimation of camera trans-  
 852 lation between two images using a camera with a 3d orientation  
 853 sensor. In *Pattern Recognition, 2002. Proceedings. 16th Interna-*  
 854 *tional Conference on*, volume 1, pages 275 – 278 vol.1, 2002.

- 855 [12] Oliver J. Woodman. An introduction to inertial navigation.  
856 Technical Report UCAM-CL-TR-696, University of Cambridge,  
857 August 2007.
- 858 [13] Richard J. Radke. *Computer Vision for Visual Effects*. Cam-  
859 bridge University Press, 2013.
- 860 [14] Ioannis M. Rekleitis. Steerable filters and cepstral analysis for  
861 optical flow calculation from a single blurred image. In *In Vision*  
862 *Interface*, pages 159–166, 1996.
- 863 [15] Jianbo Shi and Carlo Tomasi. Good features to track. In *1994*  
864 *IEEE Conference on Computer Vision and Pattern Recognition*  
865 (*CVPR'94*), pages 593 – 600, 1994.
- 866 [16] Yu-Wing Tai, Hao Du, M.S. Brown, and S. Lin. Image/video  
867 deblurring using a hybrid camera. In *Computer Vision and*  
868 *Pattern Recognition, 2008. CVPR 2008. IEEE Conference on*,  
869 pages 1–8, June 2008.
- 870 [17] Li Zhang, T. Portz, and Hongrui Jiang. Optical flow in the pres-  
871 ence of spatially-varying motion blur. *2013 IEEE Conference on*  
872 *Computer Vision and Pattern Recognition*, 0:1752–1759, 2012.